Trustworthy and Intelligent COVID-19 Diagnostic IoMT through XR and Deep Learning-based Clinic Data Access

Yonghang Tai, Bixuan Gao, Qiong Li, Zhengtao Yu, Chunsheng Zhu, Victor Chang

***Abstract*—This paper presents a novel XR and Deep Learning-based IoMT solution for the COVID-19 telemedicine diagnostic, which systematically combines VR/AR remote surgical plan/rehearse hardware, customized 5G cloud computing and deep learning algorithms to provide real-time COVID-19 treatment scheme clues. Compared to existing perception therapy techniques, our new technique can significantly improve performance and security. Our newly developed system collected 347 positive and 2270 negative COVID-19 patient clinic data from the Red Zone by 5G transmission, a novel ACGAN-based intelligent prediction algorithm is addressed to learn a new COVID-19 prediction model. The Copycat network is then employed for the model stealing and attack for the IoMT model to develop the security performance. To simplify the user interface and achieve excellent user experience, we combined the Red Zone's guiding images with the Green Zone's view through the AR navigate clue by using 5G. Furthermore, an XR surgical plan/rehearse framework is designed, including all COVID-19 surgical requisite details that were developed with a real-time response guaranteed. We have conducted a number of objective and subjective experiments for performance evaluation. Our evaluation results demonstrated that our new IoMT outperforms the existing perception techniques with significantly higher accuracy. This study suggests a new framework in the COVID-19 diagnostic integration and opens the new research about the integration of XR and deep learning for IoMT implementation.**

***Index Terms*—IoMT, COVID-19, XR, ACGAN, Security**

I. INTRODUCTION

To date, the Internet of Medical Things (IoMT) technology has been recognized and widely applied due to its high performance and practicality. The IoMT enables the application of deep learning for automated and accurate prediction of many diseases, assisting and facilitating effective and efficient medical treatment[1]-[3]. However, there are fewer studies that investigate the diagnostic IoMT through telemedicine and deep learning-based attacks targeting the services deployed on the IoMT devices, particularly the IoMT-based AI services. Since the Extended Reality (XR) technology, which includes the Virtual Reality (VR), Augmented Reality (AR) and the Mixed Reality (MR) [4]-[6], refer to the real/virtual environments generated by computer graphics and wearables has been widely applicated in the medical field, especially in the telemedicine implementations.

During outbreak of pandemic of COVID-19, IoMT can even be used to detect main symptoms ubiquitously, by the data collection from the infected area and customized the treatment plan based on aggregated IoMT data. Inspired by the aforementioned approaches, the XR implementation is introduced into the COVID-19 Diagnostic IoMT. Furthermore, a customized XR-enabled COVID-19 surgical planning/rehearse strategy is also being developed. Taking into account the previously mentioned deep learning-based IoMT platform, a novel deep neural network algorithm has been developed to predict the COVID-19 is positive or not by data 5G data transformation. Apart from that, to achieve a better human ergonomics performance, we visualized all the COVID-19 diagnostic clues from our XR surgical decision system. Thirdly, we used a Copycat-based access control system to protect the patient's clinic data used for rendering the XR images. We adopted a simplified approach based on Wang D [7], which allows electronic medical data to be accessed and shared on cloud storage. More specifically, each visit request to any patient's clinic data will be recorded into the customized 5G cloud together with a timestamp, requestor's ID, patient ID and image ID.

Three original contributions are presented in this paper:

1. For the first time, the deep ACGAN-based prediction and telemedicine surgical guiding methods are proposed for the COVID-19 diagnostic with 5G IoMT, which supplemented the shortage of medical staff and treatment of the Red Zone.

2. Copycat ACGaN is employed to steal and attack for the IoMT model to evaluate the security performance. The privacy of COVID-19 patients has been guaranteed during IoMT data transmission.

3. A novel XR-based COVID-19 surgical plan/rehearse prototype has been implemented for evaluating the new

This work was supported by the National Natural Science Foundation of China (62062069, 62062070, and 62005235).

Yonghang Tai, Qiong Li are with the Yunnan Key Laboratory of Opto-electronic Information Technology, Yunnan Normal University, Kunming, Yunnan, China. (e-mail: taiyonghang@ynnu.edu.cn).

Bixuan Gao is now with the Taikang Tongji Hospital, Wuhan, Hubei, China.

Jun Zhang is now with the Yunnan First People's Hospital, Kunming, Yunnan, China.

Zhengtao Yu is now with the Faculty of Information Engineering and Automation, Kunming University of Science and Technology, Kunming, Yunnan, China (e-mail: ztyu@hotmail.com).

Victor Chang is now with the Teesside University, UK (e-mail:victorchang.research@gmail.com)

techniques and ideas. This work opens new research on the integration of XR and deep learning for tele-surgical applications.

II. Related Work

A. XR-based Implementations for IoMT

In order to promote doctors to acquire more information conveniently during the operation, the XR-based IoMT strategy has been evaluated, which is the first method abovementioned, to rebuild the three-dimensional virtual patient from the medical images and superimpose it on the real patient in an operating room for the 3D surgical guiding [8], [9], [10]. A traditional XR system includes two steps – three-dimensional reconstruction of anatomically based on CT/MRI images and the registration step between the reconstructed model and the patient [11]. Although existing communal or software could automatically complete the three-dimensional rebuilt step, for example, the Osirix, the Mimics, and the 3D slicer, the semi-automatic manual correction by the professional surgeon, is still the most reliable strategy in the clinic applications [12]. The Curve (Brain Brainlab AG, Germany) system [13] and the Stealth Station are designed to XR navigation of MIS [14]; the NavSuite3 (Stryker Corporation, USA) is designed for the spine surgery [15]; the Navigation Panel Unit (Storz, Germany) is used for the endoscopic surgical navigation [16]; and SCOPIS (Scopis, Germany) [17], with the aid of Microsoft HoloLens, provides ENT, CMF, neuro, and spine navigation. Nevertheless, the critical issues of these commercial systems are implemented with either visual-guide or optical-guide mechanisms. In other words, the infrared-based NDI Polaris is the vital unit supporting all of these navigation schemes. Unfortunately, two serious challenges still need to be addressed for the NDI Polaris system: firstly, a precise registration between the 3D static image-based reconstructed model and the real patient is the most challenging issue due to the medical image caused by the human respiration. Furthermore, the heterogeneity of the lesions; secondly, the IR-based navigation is usually limited by the disadvantage of the signal blocking during the real operations, surgeons' operation area should not occlude the infrared transmit trajectory which also leads many inconveniences in IoMT. To the best of our knowledge, in the operation room, a majority of XR guiding surgical applications focus on the medial image fusion algorithms and the routing planning. Research has not yet introduced many intuitive perceptions, such as tactile feedback through the 5G transmission, which would significantly improve the accuracy of the surgical performance.

B. AI-based COVID-19 IoMT Platform

COVID-19 systems can quickly diagnose COVID-19 pathogens and found different types of attacks. In addition, DL Inference models were tested. Including acoustic emission disturbances to the classifier, launching a black box attack using the Clarifai REST API model, and using the back door attack to update the model [18]. Gregory B. Rehm developed a research-centric CDSS. The device leverages the power of the Internet of Things to collect real-time physiological data from patients on ventilators and other medical devices. To monitor and manage the conditions of patients in intensive care units, doctors can prioritize their care, aiming to improve diagnosis, prediction, and event recognition in intensive care units. Additionally, encrypted files are used to ensure the safety of patient information [19]. Chen designed a chronic kidney disease prediction system based on the Internet of Things (IoMT) platform, an adaptive hybridized deep convolutional neural network. CT image data from renal cancer were used and the missing values were processed with median estimates. The dual training method of learning and activation mechanisms can effectively avoid kidney disease. [20] Lalit Garg has designed and proposed a new privacy anonymous internet of things model. Moreover, an RFID proof-of-concept is provided for this model. The blockchain is used to simulate contract deployment and function execution. The model will make it easier to identify groups of infected contacts and provide mass isolation while protecting individual privacy.[21] Vinay Chamola et al. conducted detailed research on the Internet of Things, drones, blockchain, artificial intelligence and 5G. During the COVID-19 epidemic, the medical internet of things can effectively collect, analyze and transmit clinical data. Drones ensure minimal human interaction and can also be used to reach areas that are unreachable by humans. Robots and autonomous vehicles have also contributed significantly to the field of automatic disinfection by reducing human contact. Artificial intelligence plays an important role in risk prediction and prognosis treatment. [22][23]

C. Cyber-attacks with Deep Learning Network

When it comes to the Internet of Medical Things (IoMT), we should know that there is a very close connection between IoMT and the IoT. An idea was put forward by Fang Hu that IoMT could be used in the medical industry must be a truth [24]. After five years, a healthcare monitoring system had been made by V.Jagadeeswari [25] using big data training. Which proved the idea, which put forward by Fang Hu had become a truth. Nowadays, with an increasing number of cyber-attacks have appeared, Talon Flynn [26] discover that IoMT system based on a mobile platform is very easy to be breached by various network attacks. A series of evidence can be presented to support our attack model. Deep learning has gained prominence in many field, including computer vision and cybersecurity such as vulnerability detection [27, 28]. In 2014, however, Szegedy [29] and follow-up studies [30] demonstrated that small changes to the data as images are entered can attack deep learning techniques. Subsequently, Dalvi [31], Meek and Lowd [32] have proved that in the linear classification of spam detection

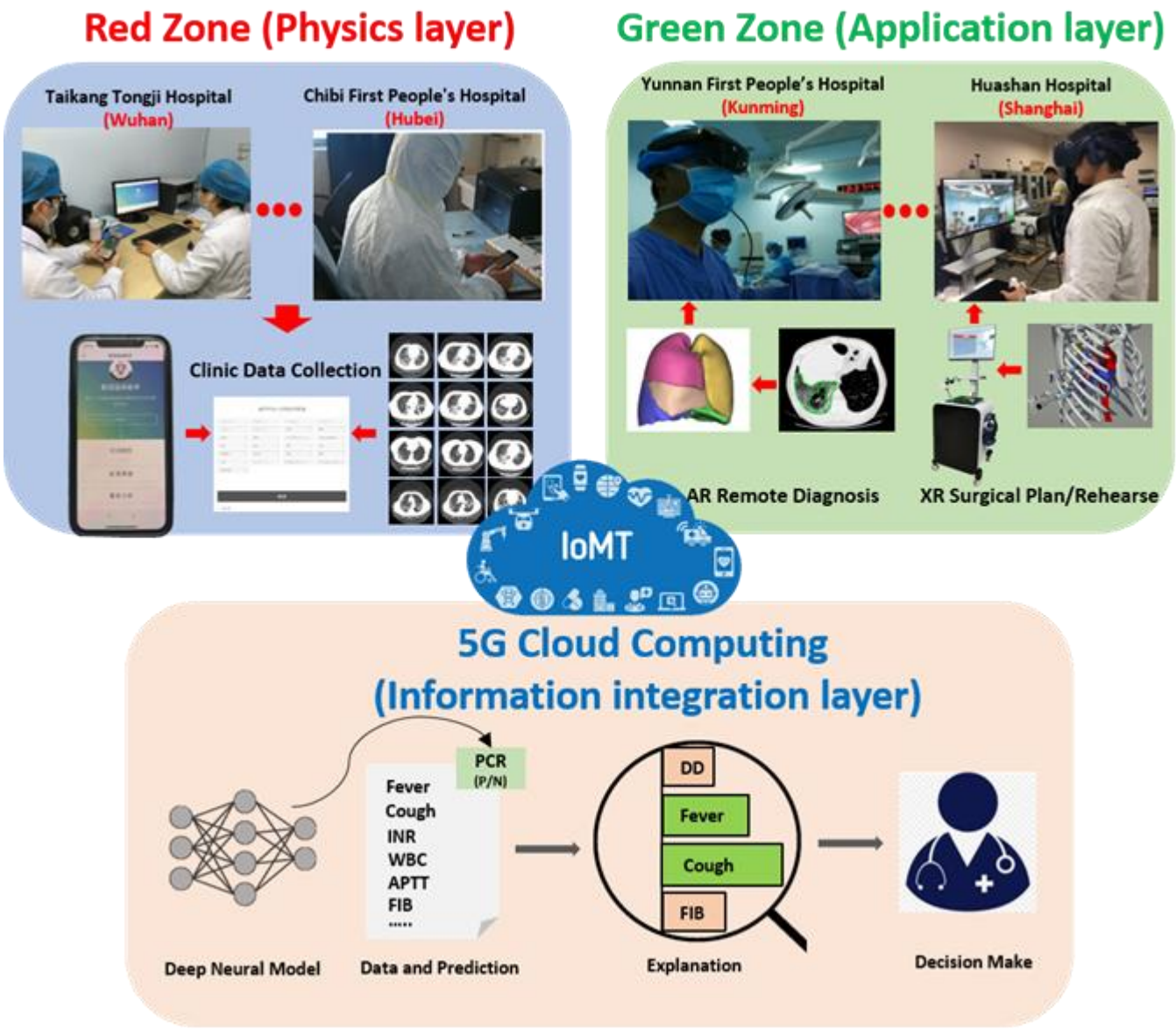

Fig. 1. Customized design of COVID-19 Diagnostic IoMT through XR and Deep Neural Model, which has been implemented in the prevention and treatment of COVID-19 in China. The Red Zone is an epidemiological term, which means the COVID-19 infected area, especially in Wuhan and Hubei. Clinic data is collected from the OPC of Red Zone by the cell phone, tablet and laptop. After that, the 5G transmission is employed to transfer and compute the medical data for the COVID-19 prediction using the 5G cloud (Alibaba Cloud). Finally, the professional respiratory physician, and the thoracic surgeon from the Green Zone, such as Shanghai and Kunming, could make a diagnosis and detailed surgical plan through the IoMT application layer with high efficiency and safety.

can be fooled by adversarial simples. Barreno et al. [33] pointed out that with the development of cyberattacks, both ML algorithms and DL algorithms can be attacked by a malicious adversary. It can be seen from the relevant literature that there are three different attack modes of adversarial attack, including white-box attack, grey box attack and black box attack. The difference between them is how much is known about the target model (including data sets, parameters/hyperparameters, deep learning models and algorithms). Because of the similarity of COVID-19 text data, among the many ways of adversarial attacks, the one that can have the most impact on our network is the grey box attack. Crafted adversarial samples have been used against a Deep Neural Network (DNN), aiming to create confrontation examples by approaching the decision boundary of the target DNN [34].

III. New System Design

In this section, we addressed the COVID-19 Diagnostic IoMT through XR and Deep Neural Model design and implementation, as demonstrated in Fig.1. A new KNN based ACGAN model is developed to estimate the COVID-19 prediction accuracy and the XR platform is employed for the remote diagnoses. After that, the 5G transmission is employed to transfer and compute the medical data for the COVID-19 prediction using the 5G cloud. AR-remote diagnose and XR surgical implementations is developed, we also present the evaluation approaches, which evaluate the performances with different kinds of deep neural algorithms.

A. ACGAN-based COVID-19 intelligent network design

The whole technological process of the ACGAN-based COVID-19 intelligent prediction system is demonstrated in Fig.2. The real-world clinical data is collected and then some preprocessing, including samples wrangling (such as selecting the demanding data and setting correct data formats), KNN for missing data imputation and resampling techniques for solving the problem of imbalance samples between normal subjects and COVID-19 subjects in a retrospective cohort. The processed training set is employed to train the ACGAN prediction model. After that, the well-trained discriminator of ACGAN is used to forecasting the samples from the prospective cohort. Finally, the interpretability of this system is produced by CEM to give an analysis of medical significance. The further descriptions of each part of ACGAN-based COVID-19 intelligent prediction are provided as follow.

1) KNN for Missing Data Imputation

A technique widely-used for handling with the extremely imbalanced distribution of samples is regarded as resampling. In resampling, to make up for the imbalanced class, a bias is used for reselecting more samples from one class which has smaller number of data than another type. The process of resampling has mainly consisted of the two parts: deleting some samples from the majority class, which is called under sampling, and augmenting samples from the minority class which is called oversampling.

Due to the influence of elements such as broken system and man-made error, the missing of recording clinical data is inevitable. Moreover, much worthwhile information on the original data would be loss resulting in the decreases of forecasting accuracy and the mistaken research result, if only to delete these missing data. In this work, k-nearest neighbour (KNN)-based missing data estimation algorithm is utilized to solve this thorny problem. In the KNN, the k samples nearest to the missing sample are searched from all complete instances in the dataset, and then the corresponding missing value is padded with the mean value of these using the mean value samples. In KNN, the (X, Y, Z) is defined as the features of samples, and then their k nearest neighbors are $D_k = \{(X_k, Y_k, Z_k) | j = 1, 2, \dots, k\}$. The KNN estimator can be described as follow:

$$Y = \arg\max_v \Big(\sum_{(X_k, Y_k, Z_k) \in D_k} C(Y_j = n) \Big)$$

where X_k is the target sample, Y_j is a missing feature in X, Z_k is the classification which is 0 or 1 in the current task, n represents the value within the range of the Y and $C(Y_k = n)$ represents a discriminant function that outputs 0 or 1 depending on its argument is false or true.

In order to choose the k samples nearest to the target sample, the similarity between the target sample and the corresponding k nearest samples must be minimum. And the commonly-used approach called Minkowski distance (or its variants) is given as follows,

$$Dis(i,j) = \sqrt[q]{|x_{i1} - x_{j1}|^q + |x_{i2} - x_{j2}|^q + \cdots + |x_{ip} - x_{jp}|^q}, (x_{ip} \in X_i, x_{jp} \in X_j)$$

Where q represents a positive integer which is the Minkowski coefficient. Minkowski distance is defined as Manhattan distance, when $q = 1$ and it described as Euclidean distance when $q = 2$. In the current system, the $q = 1$ is used.

2) Deep Training Module Design

Deep learning techniques are widely used in medical application, prediction, and retrieval domains, promising very good performance in classification fields. The Auxiliary Classifier Generative Adversarial Networks (ACGAN) is was further improved on the basis of the CGAN through incorporation of the idea of mutual information in InfoGAN [35]. Unlike traditional generative networks which are based on the unsupervised models, the supervised learning method is used in the generated adversarial concept. Furthermore, the internal structure of ACGAN adds the portion embedding the class information into the input of generater and compared with traditional CGAN. The additional task for ACGAN is to classify the category of samples by expanding an auxiliary judgement layer in discriminator which can output the class labels of input samples [36]. Due to the speciality of the network, the objective function of ACGANs is divided into two part: the log-likelihood of the correct source L_S and the log-likelihood of the correct class L_C.

$$L_S = E[\log p\,(s = real | X_{real})] + E[logp(s = fake | G(z))]$$
$$L_y = E[\log p\,(Y = y | X_{real})] + E[logp(Y = y | G(z))]$$

Where g represents the created clinical sample. The discriminator D is trained to find the maximum of L_S+L_y, while the generator is trained to find maximum of $L_Y - L_S$.

3) Contrastive explanations method for prediction system

Contrastive explanations method (CEM) is an AI novel algorithm created and implemented by IBM research, which that can provide contrastive explanations for black box models such as deep neural networks well-known as black box models. CEM can be effectively used to create meaningful explanations in different domains that are presumably easier to consume as well as more accurate [37]. CEM of looking for the correlation positive/negative is expressed as an optimization problem of using perturbation variable δ that is used to explain how the model's deep learning model to decide prediction results according to the input features. In finding pertinent negatives (PN), X is defined as the feasible data; (x_0, y_0) $x_0 \in X$ is an example where y_0 is the class label predicted by a neural network model; $x \in X$ is a modified example which is defined as a perturbation variable δ applied to x_0: $x = x_0 + \delta$ and y_δ is the corresponding prediction results. For any natural example x, CEM dedicates to find an interpretable perturbation and thus study the difference between the $argmax_i[Pred(x_0)]_i$ and $argmax_i[Pred(x_0 + \delta)]_i$ where $Pred(\cdot)$ is the output consisting of prediction probabilities for all classes. The implementations of CEM finding PN are formulated as follow:

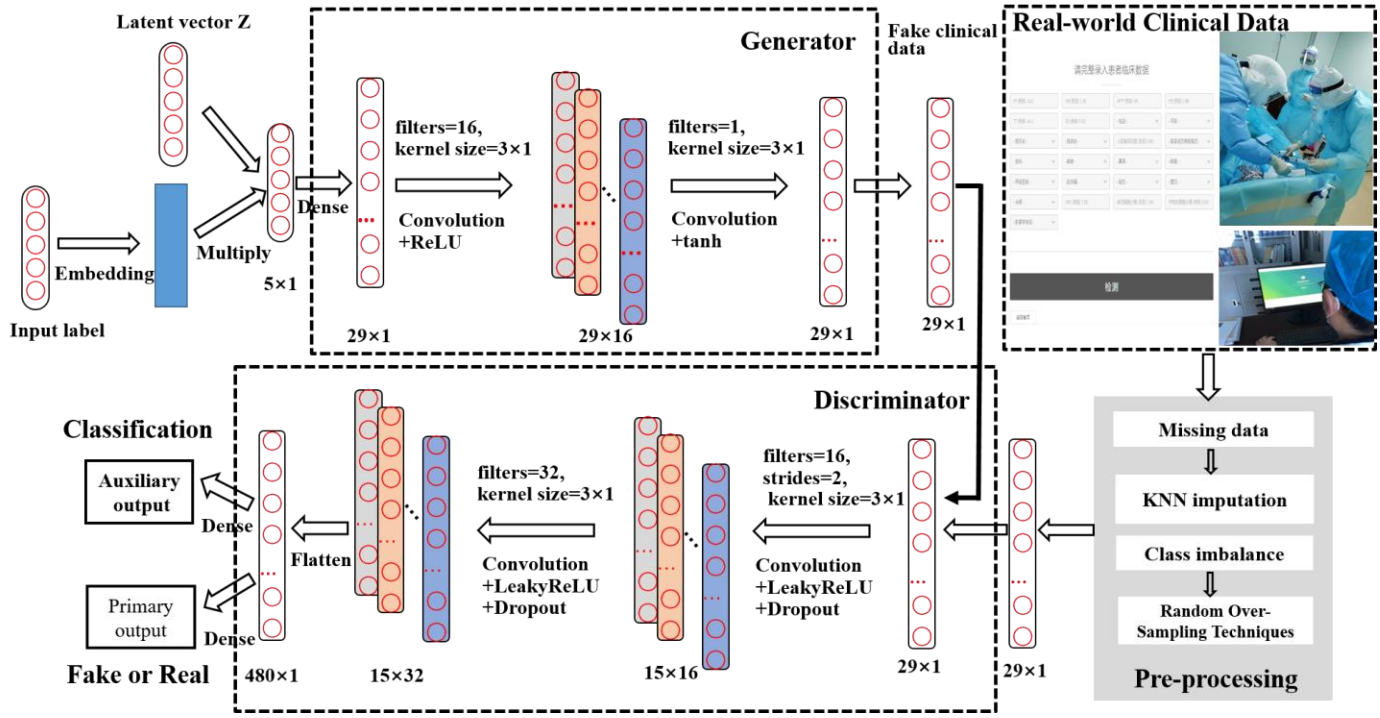

Fig. 2. The ACGAN-based COVID-19 intelligent prediction network: the real-world clinical data is collected, and then some preprocessing including samples wrangling (such as selecting the demanding data and setting correct data formats), KNN for missing data imputation and resampling techniques for solving the problem of imbalance samples between normal subjects and COVID-19 subjects in a retrospective cohort. The processed training set is employed to train the ACGAN prediction model. After that, the well-trained discriminator of ACGAN is used to forecasting the samples from a prospective cohort. Finally, the interpretability of this system is produced by CEM to give an analysis for medical significance.

$$\min_{\delta \in X/x_0} c \cdot f_k^{neg}(x_0,\delta) + \beta \|\delta\|_1 + \|\delta\|_2^2 + \gamma \|x_0 + \delta - AE(x_0+\delta)\|_2^2$$

Where $f_k^{neg}(x_0,\delta)$ is an objective function designed to encourage x to be predicted as a different class than $y_0 = arg\,max_i [Pred(x_0)]_i$. $[Pred(x_0,\delta)]_i$ represents the i-th class probabilities of x, k refers to confidence parameter controlling the separation between $[Pred(x)]_{y_0}$ and $\max_{i \neq t_0} [Pred(x)]_i$, $\beta\|\delta\|_1$ and $\|\delta\|_2^2$ called elastic net regularizer, which is used for efficient feature selection in high-dimensional learning problems [38]. $\|x_0 + \delta - AE(x_0+\delta)\|_2^2$ is an L_2 reconstruction error of x evaluated by auto encoder, c, β and γ are the associated regularization coefficients.

B. *XR-Based COVID-19 remote diagnosis platform.*

1) *COVID-19 Patient-specific CT 3D Rendering*

The CT images for the visual rendering are provided by the hospital in Fig. 4 show some examples of images. The sample case for the clinical stage is a 55-year old male presented to the hospital in Kunming. He had a two days history of pharyngalgia, headache, rhinorrhea and fever. He did not contact any COVID-19 patients. Apart from a history of hypertension, the patient was a 30-year smoker. The patient's chest CT scan (February 8, 2020) demonstrated the unilateral peripheral distribution of ground-glass opacities, as shown in Fig.4. Laboratory investigations illustrated that elevated white blood cell count (3.62×109/L, normal range, 4-10×109/L), higher count of neutrophil (9.2×109/L, normal range, 2.0-7.5×109/L) and lymphocyte count was slightly reduced at 0.42×109/L (normal range 0.8-4.0×109/L). Firstly, we imported patients' CT images, the DICOM format, to reconstruct a surgical simulation demo. Four professional thoracic surgeons manually corrected the COVID-19 infection region of interest after that, which is demonstrated in the third column of Fig. 3. The 3D mesh reconstructed model is used in the marching cube algorithm. We programmed the process of using the SDK such as VTK, CTK, ITK, IGSTK, for the visual rendering. Finally, we employed the shade programming to paint on the vertex colors. The virtual patient was characterized by transparency, variable size, and enabling the trainees to monitor their surgical operation visually. Various triggers are implemented to respond to the surgical tools touching different COVID-19 lung demo layers that help judge which costa will be punctured by the trocar needle inserting the current route.

2) *XR surgical Visual-haptic Implementation*

The VATS-XR systems developed in this article mainly include the development of hardware and software. Fig. 3. shows the framework of the system. The tactile and visual are two important indicators of the system. For visual aspects, the OpenHaptic plugin calls feedback devices to interact with virtual objects, such as collision detection and soft tissue cutting and deformation. For visual elements, interactive objects are rendered more realistically by shader language, to make it close to the real physical model. UGUI is used to design the UI interface design of the system. These functions were finally implemented in Unity3D. Surgical instruments and force feedback devices are connected through the linker. The operator

holds the surgical instrument to bring the three axes of the power feedback device to perform corresponding transformation operations. When the clip of the virtual surgical instrument interacts with the virtual object, computer calls the force feedback device through the OpenHaptic plugin (Geomagic, USA) to give the corresponding driving force, thereby giving the operator a real tactile sense. HTC VIVE and Logitech camera are used to realize XR display methods.

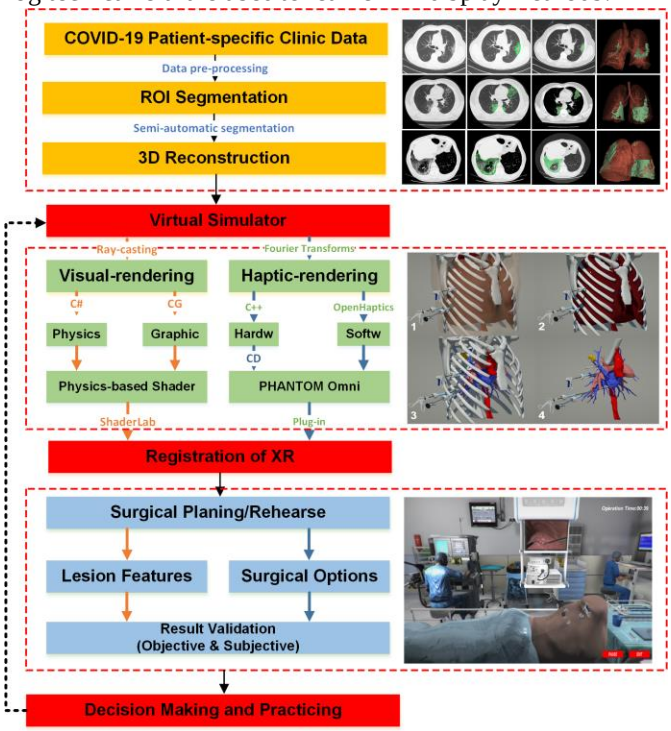

Fig. 3. XR COVID-19 surgical IoMT simulator framework: the first part is the COVID-19 patient-specific medical image processing from the clinic data collection. The second part is the XR visuo-haptic reconstruction with the medical data. The third part is the audio rendering procedure, stored the audio details of OR-based heart monitor, anesthesia and breathing apparatus and line four is the surgical environment reconstruction.

3) 3DUI Design

Referring to the GPS navigation interface, we developed a Haptic-XR based 3DUI with the XR device and the main parts of the UI included in both visual and haptic intro-operation details. Three main kinds of XR display technologies during the operation have been presented; compared to the video-based and projection-based XR navigation system, the see-through display system using a semi-transparent free-form lens to reflect the digital content overlapped with the patient on the near-eye micro-display provided an intuitional and portable surgical experience. In this paper, we chose the see-through XR display pattern with the Microsoft HoloLens mixed reality head-mounted display (HMD). Since the C-arm image or ultrasound image is the most essential navigational clues during the intentional surgery, we put the real-time CT images on the central left part of the 3DUI, as demonstrated in Fig 5. For the real-time XR, the navigation interface is constructed in the top right of the UI, which is the manipulation platform for the Haptic-XR surgical simulator. We introduced this module to mimic the real operation in OR. Apart from these two components, the coronal, sagittal and axial CT images synchronously display the needle track during the surgical simulation as a part of XR navigation. Referring to the GPS interface, we integrated the navigation clues in the bottom of the 3DUI, which includes the operation time, intervention depth, force limitation, speed limitation, the matching layer of the tissue, and the warning of mis-puncture during the surgery, as demonstrated in the bottom of Fig. 4.

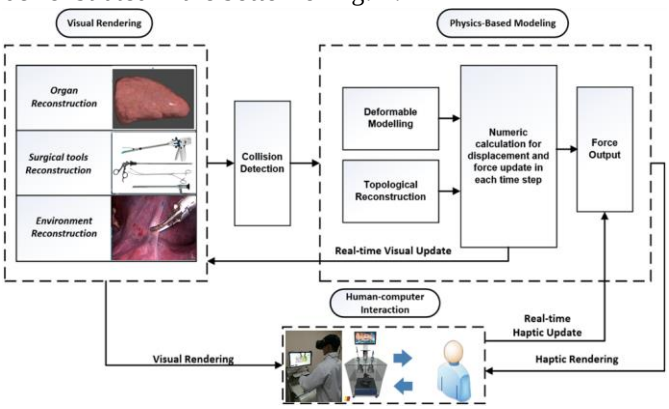

Fig. 4. Diagram of the general software architecture of the Haptic-XR based 3DUI with the IoMT device integrative implementation.

C. Model Stealing Attack to The New IoMT Platform

In this section, we'll show you how to train an imitation network (Copycat network) by stealing labels from the original network (Auxiliary Classifier GANs). In this paper, model stealing attacks mainly use the fake natural dataset to steal labels from the ACGAN and put these labels and the dataset into the imitation network. From Fig.4, we can conclude that this process mainly consists of two steps. The first step is to create a training dataset that has a similar structure to the original dataset, but they come from different problem domains (PD). So, the dataset we have chosen is different from the original dataset. Obviously, in the second step, we must use the labels and the pseudo dataset to train our model (In this paper, we choose the ACGAN as a copycat model.).

Even though the dataset obtained from the first-line hospital is used in the original network, we can still download a similar COVID-19 dataset from the Internet and then change its data structure to have a similar structure with the original dataset. By doing this, we can be stealing the corresponding label from the original model.

Next, we will explain the assignability of adversarial samples. Suppose that the adversary is interested in classifying the wrong sample and producing a hostile sample $\overrightarrow{\omega^*}$ different from the model in which the class is assigned to the legal input $\vec{\omega}$. In the following optimization formula, we can achieve this:

$$\overrightarrow{\omega^*} = \vec{\omega} + \theta_{\vec{\omega}} \text{ where } \theta_{\vec{\omega}} = arg\min_{\vec{\alpha}} g(\vec{\omega} + \vec{\alpha}) \neq g(\vec{\omega})$$

Misleading example $\overrightarrow{\omega^*}$, deliberately g calculation model. However, adversarial samples are often incorrectly classified as g' instead of g in practice. For the convenience of discussion, the concept of transferability of adversarial samples is formalized:

$$\Pi_Y(g, g') = |\{g'(\vec{\omega}) \neq g'(\vec{\omega} + \overrightarrow{\theta_{\vec{\omega}}} : \vec{\omega} \in Y)\}|$$

Set Y represents expected input distribution solved by the model g and g'. in the task. We divide the transferability of adversarial samples into two variables to describe the models (g, g'). The first is the transferability within the technology.

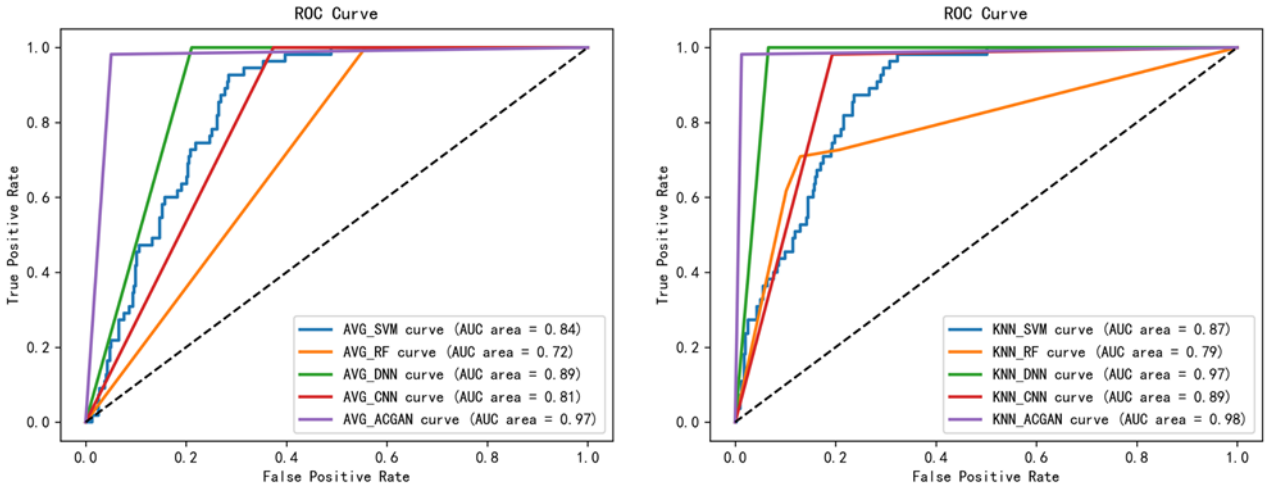

Fig. 5. The interpretation to the KNN-ACGANs with respect to how the clinical feature influences their decision for whether a patient is infected with COVID-19. It can be seen from Fig.6 that lymphocyte quantity, mitochondria quantity and whether patients have above symptoms (from fever to headache) are the top -3 risk factors affecting the model to estimate the probability of patients getting COVID-19.

The transferability between different parameter initializations of the same technology or training models of different datasets (for example, g and g' are deep learning networks or both support vector machines (SVM)) has been defined. Second, for cross-technology transferability, two technologies can be used to train models (for example, g is a deep learning network and g' is SVM).

IV. Results

A. KNN-ACGAN Learning Accuracy

Based on the prospective cohort, the results toward COVID-19 prediction for KNN-ACGAN and the other four models (KNN-SVM, KNN-RF, KNN-DNN, KNN-CNN) are reported in Table I. The evaluation metrics include Precision, Recall and F1-score. As shown in Table I, the highest values indicate that our proposed KNN-ACGAN model has the best prediction performance compared to KNN-SVM, KNN-RF, KNN-DNN and KNN-CNN.

TABLE I
PERFORMANCE COMPARISON BETWEEN THE PROPOSED KNN-ACGAN MODEL AND THE FOUR GENERAL PREDICTION METHODS

Model	Precision	Recall	F_1-score
KNN-SVM	0.75	0.98	0.85
KNN-RF	0.63	0.95	0.75
KNN-DNN	0.81	1.00	0.89
KNN-CNN	0.77	0.98	0.86
KNN-ACGAN	**0.92**	**0.98**	**0.95**

SVM: Support vector machine; RF: Random forest; DNN: Original deep neural network; CNN: Convolution neural network.

To evaluate the forecasting performance of KNN imputation for missing data, we performed a comparison between the KNN-based prediction model and the average-based prediction model. The area under the ROC curve (AUC) of the comparison result is shown in Fig. 5. In terms of ROC, KNN-based models obtain promotions compared to average-based models. Table II reports the detailed promotion of the comparison of KNN-based models and average-based models under three performance criteria. It visually shows that all KNN-based predictive models have more significant improvement in performance than KNN-based models.

TABLE II
THE PROMOTION OF KNN-BASE PREDICTION MODEL COMPARED TO AVERAGE-BASED PREDICTION MODEL IN PRECISION, RECALL AND F1-SCORE

KNN-based model vs. Average-based model	SVM	RF	DNN	CNN	ACGAN
$P_{precision}$	0.03	-0.05	0.42	0.33	0.16
P_{recall}	0.02	0.41	0.00	-0.02	0.01
$P_{f1\text{-}score}$	0.02	0.12	0.24	0.18	0.07

$$P_{criterion} = \frac{Criterion_{KNN} - Criterion_{Average}}{Criterion_{Average}}$$

B. Stealing Model Performance for the New IoMT Platform

There are some evaluation indicators and corresponding parameters shown in Table III. A higher number on the same scale indicates better performance for the model. The values Precision in the Table II are very close to 1, indicating that the original network has a strong performance in predicting COVID-19 and non-COVID-19 data.

TABLE III
VALUES OF DIFFERENT INDICATORS OUTPUTTED BY THE TARGET MODEL.

Object	Precision	Recall	F_1_score	Support
NORMAL	1.00	0.97	0.99	68
COVID-19	0.78	1.00	0.88	7
Macro avg	0.89	0.99	0.93	75
Weighted avg	0.98	0.97	0.97	75
Accuracy	—	—	0.97	75

Table III shows the different performance indicators that copycat network outputs after training with stolen labels and the corresponding dataset. Compared to the original network, the copycat network can achieve 80% similarity with the data in Table I and Table II. Because we selected data between PD and non-Problem Domain (NPD) when we selected the Copycat dataset, we still got a 79% accuracy rate with many irrelevant data effects.

TABLE IV
VALUES OF DIFFERENT INDICATORS OUTPUTTED BY THE COPYCAT MODEL.

Object(copycat)	Precision	Recall	F1_score	Support
NORMAL	1.00	0.77	0.87	196

COVID-19	0.38	1.00	0.55	28
Macro avg	0.69	0.88	0.71	224
Weighted avg	0.92	0.79	0.83	224
Accuracy	—	—	0.79	224

V. DISCUSSION

In order to develop an intelligent and trustworthy COVID-19 Diagnostic IoMT through XR and deep neural network, the XR based framework has been conducted. Based on the training results, the COVID-19 can be accomplished diagnose with or without assistance, so that visual feedback and numerical feedback are provided. Offering includes displaying a real-time 3D representation of the surgical implementations.

A. Performance by ACGAN-based COVID-19 IoMT

As shown in Table I, the proposed KNN-ACGAN model has excellent performance. Compared with the CNN model, the precision and f1-score on the KNN-ACGAN increased by 15% and 9%, respectively. Compared with the DNN model, the precision and f1-score on the KNN-ACGAN increased by 11% and 6%, respectively. It indicates that the ACGAN model can obtain more accurate features and more precise prediction results after the preprocessing of KNN for missing data and the resampling processing in training. We used KNN (k=1) to fill up the missing data and the oversampling to solve the problem of imbalance samples. In Fig. 5 and TABLE II, where the performance of KNN is evaluated, the AUC of the KNN-based models has increased by 1%-8% compared with average-based models. Moreover, except for the Pprecision of KNN-RF and the Precall of KNN-CNN, all the KNN-based models have a promotion in which Pf1-score have increased by 2%-24%, Precall have increased by 2%-41% and Pprecision have increased by 3%-41%. More promising information can be obtained from the confusion matrix in Fig 6. All the experiments demonstrate that KNN-ACGAN is a promising technology that can be used effectively in COVID-19 prediction.

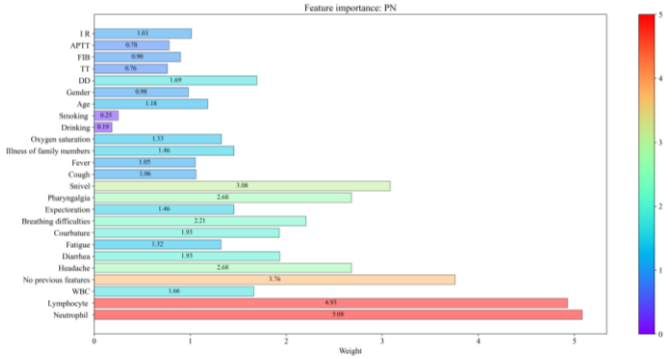

Figure 6. The interpretation of important clinical features based on the CEM algorithm.

In the offline process, we use real-world clinical COVID-19 data to train the proposed KNN-ACGAN model. After optimizing and adjusting the model parameters, the model is saved. The new experiments with the protected model are performed in the online application. According to the predicted feedback, whether the patients are infected are predicted and displayed on the monitor. Besides, the interpretability based on CEM can provide the importance for the clinical features, which gives the KNN-ACGAN model the medical insight and ensure the reliability of our proposed COVID-19 intelligent prediction system.

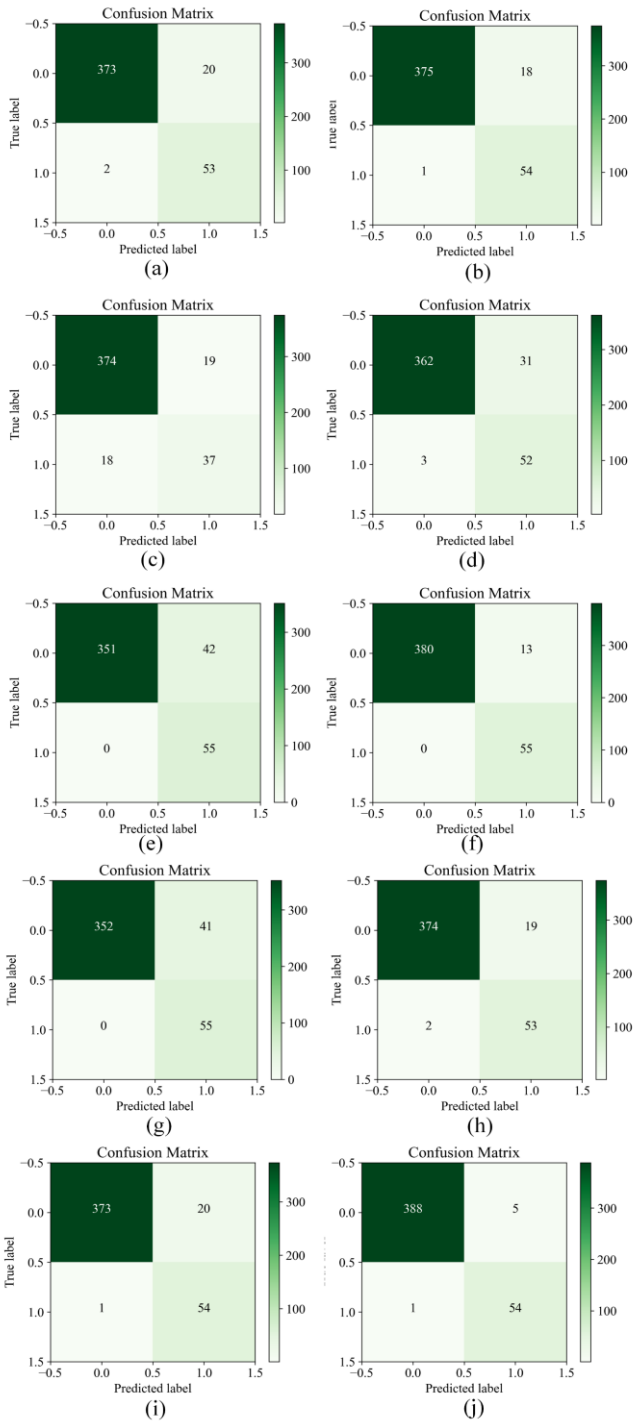

Fig. 7. The confusion matrix for different algorithms. (a) AVG-SVM, (b) KNN-SVM, (c) AVG-RF, (d) KNN-RF, (e) AVG-DNN, (f) KNN-DNN, (g) AVG-CNN, (h) KNN-CNN, (i) AVG-ACGAN, (j) KNN-ACGAN.

B. Performance by IoMT Stealing Model

As shown in Figure 9, the obfuscated matrix is an error matrix that can be used to evaluate the performance of supervised learning algorithms. Therefore, we can see more clearly that the prediction set is a mixed part of the real set through the confusion matrix. We can see from Figure 9, True Positive (TP) and False Negative (FN) account for a large proportion in the

confounding matrix, among which TP accounts for the largest proportion, which has been directly reflected that the ACGAN network can accurately predict the data of patients with and without COVID-19.

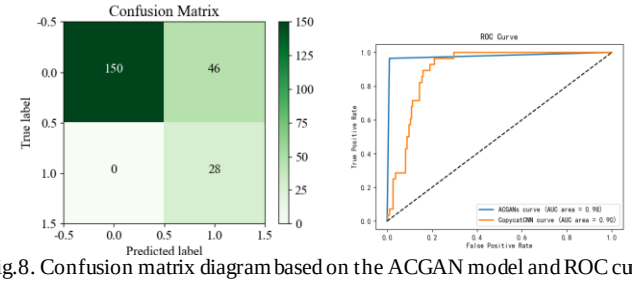

Fig.8. Confusion matrix diagram based on the ACGAN model and ROC curve using different models for data prediction.

The Receiver Operating Characteristic (ROC) curve is drawn according to a series of different dichotomies (cut-off values or determining thresholds), unlike traditional evaluation methods, the ROC curve does not need to divide experimental results into two categories for statistical analysis, and all points on the curve reflect the same receptivity. The ROC curve is judged by which line in the curve can get the fastest and most infinitely close to an ordinate of 1, indicating that the model represented by that curve will work best. As we can see from Figure, KNN-ACGAN can have the best effect on the classification of new crown data. ACGAN can more accurately predict the data of COVID-19 patients and non-COVID-19 patients by combining the results of the ROC curve and confounding matrix. At the same time, the copycat network can also achieve similar effects to the original network.

VI. CONCLUSION

In this paper, we proposed a Trustworthy and Intelligent COVID-19 Diagnostic IoMT through XR and deep neural networks. We developed a customized novel ACGAN-based intelligent prediction algorithm that was addressed to learn a new COVID-19 prediction model. Apart from that, to achieve a better human ergonomics performance, we visualized all the navigational clues from our Haptic-AR guide system. We are among the first to apply deep learning for the COVID-19 IoMT prediction and remote surgical plan cues, which may provide a new strategy for COVID-19 therapy. In the future, we will improve this IoMT system in both hardware design and deep learning algorithms promotion, aims to create a platform for both academia and industry to the COVID-19 track and treatment.

ACKNOWLEDGMENT

This research is funded by the Yunnan Key Laboratory of Opto-electronic Information Technology of Yunnan Normal University. We thank Dr. Yinjia Wang of Chibi People's Hospital for the COVID-19 clinic data collection and Dr. Kai Qian of Huashan Hospital for the COVID-19 surgical suggestions. Prof. Chang's work is partly supported by VC Research (VCR 0000113).

REFERENCES

[1] Kumar M, Chand S. A Secure and Efficient Cloud-Centric Internet of Medical Things-Enabled Smart Healthcare System with Public Verifiability[J]. IEEE Internet of Things Journal, 2020.

[2] Ding Y, Wu G, Chen D, et al. DeepEDN: A Deep Learning-based Image Encryption and Decryption Network for Internet of Medical Things[J]. arXiv preprint arXiv:2004.05523, 2020.

[3] Rahman A, Hossain M S, Alrajeh N A, et al. Adversarial Examples–Security Threats to COVID-19 Deep Learning Systems in Medical IoT Devices[J]. IEEE Internet of Things Journal, 2020.

[4] A. Elmi-Terander, H. Skulason, M. Soderman, J. Racadio, R. Homan, D. Babic, N. Van Der Vaart, and R. Nachabe, "Surgical navigation technology based on augmented reality and integrated 3D intraoperative imaging a spine cadaveric feasibility and accuracy study," *Spine (Phila. Pa. 1976).*, vol. 41, no. 21, pp. E1303–E1311, 2016.

[5] L. Li, J. Yang, Y. Chu, W. Wu, J. Xue, P. Liang, and L. Chen, "A novel augmented reality navigation system for endoscopic sinus and skull base surgery: A feasibility study," *PLoS One*, vol. 11, no. 1, pp. 1–17, 2016.

[6] M. Kersten-Oertel, P. Jannin, and D. L. Collins, "The state of the art of visualization in mixed reality image guided surgery," *Comput. Med. Imaging Graph.*, vol. 37, no. 2, pp. 98–112, 2013.

[7] Wang D, Hu B, Hu C, et al. Clinical Characteristics of 138 Hospitalized Patients With 2019 Novel Coronavirus-Infected Pneumonia in Wuhan, China. *JAMA*. 2020.

[8] U. Mezger, C. Jendrewski, and M. Bartels, "Navigation in surgery," *Langenbeck's Arch. Surg.*, vol. 398, no. 4, pp. 501–514, 2013.

[9] S. M. Krieg, J. Sabih, L. Bulubasova, T. Obermueller, C. Negwer, I. Janssen, E. Shiban, B. Meyer, and F. Ringel, "Preoperative motor mapping by navigated transcranial magnetic brain stimulation improves outcome for motor eloquent lesions," *Neuro. Oncol.*, vol. 16, no. 9, pp. 1274–1282, 2014.

[10] J. Saito, M. Kitayama, R. Kato, and K. Hirota, "Interference with pulse oximetry by the Stealth Station™ Image Guidance System," *JA Clin. Reports*, vol. 3, no. 1, p. 6, 2017.

[11] X. Chen, L. Xu, Y. Wang, H. Wang, F. Wang, X. Zeng, Q. Wang, and J. Egger, "Development of a surgical navigation system based on augmented reality using an optical see-through head-mounted display," *J. Biomed. Inform.*, vol. 55, pp. 124–131, 2015.

[12] P. K. Burduk, K. Dalke, and W. Kaźmierczak, "Intraoperative navigation system in endoscopic sinus surgery," *Otolaryngol. Pol. = Polish Otolaryngol.*, vol. 66, no. 4 Suppl, pp. 36–9, 2012.

[13] M. J. Citardi, W. Yao, and A. Luong, "Next-Generation Surgical Navigation Systems in Sinus and Skull Base Surgery," *Otolaryngologic Clinics of North America*, vol. 50, no. 3. pp. 617–632, 2017.

[14] D. Ni, W. Y. Chan, J. Qin, Y. P. Chui, I. Qu, S. S. M. Ho, and P. A. Heng, "A virtual reality simulator for ultrasound-guided biopsy training," IEEE Comput. Graph. Appl., vol. 31, no. 2, pp. 36–48, 2011.

[15] S. Y. Selmi, G. Fiard, E. Promayon, L. Vadcard, and J. Troccaz, "A virtual reality simulator combining a learning environment and clinical case database for image-guided prostate biopsy," in Proceedings of CBMS 2013 - 26th IEEE International Symposium on Computer-Based Medical Systems, 2013, pp. 179–184.

[16] N. Yi, X. J. Guo, X. R. Li, X. F. Xu, and W. J. Ma, "The implementation of haptic interaction in virtual surgery," in Proceedings - International Conference on Electrical and Control Engineering, ICECE 2010, 2010, pp. 2351–2354.

[17] L. Wei, Z. Najdovski, W. Abdelrahman, S. Nahavandi, and H. Weisinger, "Augmented optometry training simulator with multi-point haptics," Conf. Proc. - IEEE Int. Conf. Syst. Man Cybern., pp. 2991–2997, 2012.

[18] Holshue ML, DeBolt C, Lindquist S, et al. First Case of 2019 Novel Coronavirus in the United States. *N Engl J Med*. 2020.

[19] Chan JF, Yuan S, Kok KH, et al. A familial cluster of pneumonia associated with the 2019 novel coronavirus indicating person-to-person transmission: a study of a family cluster. *Lancet*. 2020.

[20] Rehm G B, Woo S H, Chen X L, et al. Leveraging IoTs and Machine Learning for Patient Diagnosis and Ventilation Management in the Intensive Care Unit. IEEE Pervasive Computing, 2020.

[21] Chamola V, Hassija V, Gupta V, et al. A Comprehensive Review of the COVID-19 Pandemic and the Role of IoT, Drones, AI, Blockchain, and 5G in Managing its Impact. IEEE Access, 2020, 8: 90225-90265.

[22] Chen G, Ding C, Li Y, et al. Prediction of Chronic Kidney Disease using Adaptive Hybridized Deep Convolutional Neural Network on the Internet of Medical Things Platform[J]. IEEE Access, 2020.

[23] Garg L, Chukwu E, Nasser N, et al. Anonymity preserving IoT-based COVID-19 and other infectious disease contact tracing model. IEEE Access, 2020.
[24] Hu F, Xie D, Shen S. On the application of the internet of things in the field of medical and health care[C]//2013 IEEE international conference on green computing and communications and IEEE Internet of Things and IEEE cyber, physical and social computing. IEEE, 2013: 2053-2058.
[25] Jagadeeswari V, Subramaniyaswamy V, Logesh R, et al. A study on medical Internet of Things and Big Data in personalized healthcare system. Health information science and systems, 2018, 6(1): 14.
[26] Flynn T, Grispos G, Glisson W, et al. Knock! knock! who is there? investigating data leakage from a medical internet of things hijacking attack[C]//Proceedings of the 53rd Hawaii International Conference on System Sciences. 2020.
[27] Gu J, Wang Z, Kuen J, et al. Recent advances in convolutional neural networks[J]. Pattern Recognition, 2018, 77: 354-377.
[28] Nan Sun, Jun Zhang, Paul Rimba, Shang Gao, Leo Yu Zhang and Yang Xiang, "Data-driven Cybersecurity Incident Prediction: A Survey," IEEE Communications Surveys and Tutorials, vol. 21, no. 2, pp. 1744-1772, 2019.
[29] Szegedy C, Zaremba W, Sutskever I, et al. Intriguing properties of neural networks[J]. arXiv preprint arXiv:1312.6199, 2013.
[30] Goodfellow I J, Shlens J, Szegedy C. Explaining and harnessing adversarial examples[J]. arXiv preprint arXiv:1412.6572, 2014.
[31] Dalvi N, Domingos P, Sanghai S, et al. Adversarial classification[C]//Proceedings of the tenth ACM SIGKDD international conference on Knowledge discovery and data mining. 2004: 99-108.
[32] Lowd D, Lowd D. Adversarial learning[C]//Proceedings of the eleventh ACM SIGKDD international conference on Knowledge discovery in data mining. 2005: 641-647.
[33] Barreno M, Nelson B, Sears R, et al. Can machine learning be secure[C]//Proceedings of the 2006 ACM Symposium on Information, computer and communications security. 2006: 16-25.
[34] Bapiyev I M, Aitchanov B H, Tereikovskyi I A, et al. Deep neural networks in cyber attack detection systems[J]. International Journal of Civil Engineering and Technology (IJCIET), 2017, 8(11): 1086-1092.
[35] P. Salehi, A. Chalechale, and M. Taghizadeh, "Generative Adversarial Networks (GANs): An Overview of Theoretical Model, Evaluation Metrics, and Recent Developments," 2020.
[36] A. Odena, C. Olah, and J. Shlens, "Conditional image synthesis with auxiliary classifier gans," in *34th International Conference on Machine Learning, ICML 2017*, 2017, vol. 6, pp. 4043–4055.
[37] B. Erol, S. Z. Gurbuz, and M. G. Amin, "Motion Classification Using Kinematically Sifted ACGAN-Synthesized Radar Micro-Doppler Signatures," *IEEE Trans. Aerosp. Electron. Syst.*, vol. 56, no. 4, pp. 3197–3213, 2020.
[38] A. Dhurandhar *et al.*, "Explanations based on the Missing: Towards contrastive explanations with pertinent negatives," in *Advances in Neural Information Processing Systems*, 2018, vol. 2018-Decem, no. NeurIPS, pp. 592–603.